Contributions to Prototype Dark Matter Experiments

I. Rydstrom
Santa Clara University Department of Physics
500 El Camino Real, Santa Clara, CA 95053

June 12, 2024

Abstract In this thesis, I summarize my contributions to prototype dark matter experiments performed at SLAC National Accelerator Laboratory under the direction of Prof. Betty Young and Dr. Noah Kurinsky. I begin with a brief introduction to the dark matter problem, solid-state low temperature detectors, and the cryostats I learned to operate as part of my research. I then describe my contributions to a new prototype dark matter experiment underway at SLAC known as SPLENDOR, sample imaging performed on microwave kinetic inductance detectors, and the development of a custom graphical user interface for cryostat control. **Keywords**: *Low Temperature Detectors, Superconductivity, Dark Matter.*

1 Introduction & Motivation

1.1 The Dark Matter Problem

Historically, the cosmos have been one of mankind's most deeply studied frontiers. For hundreds of years, astronomers have pointed their telescopes in the direction of the skies to seek insight on many great mysteries of the universe and how we got here. Largely, the greatest breakthroughs in astronomy have been limited by the technology available to astronomers at the time. From the era of early astronomy and the first optical telescopes, to the modern era of complex superconducting focal planes that exploit quantum phenomena, it is seen that our ability to study the universe is directly correlated with the technology available to scientists at the current time. Today, we live in a time of great technological maturity, promising extraordinary progress in our longest-standing unsolved problems. Dark matter is one such problem now being pushed forward due to advances in rare-event detector technology.

The true nature of dark matter is ultimately unknown. Its premise dates back several decades to the first indirect sources of evidence, some of which used discrepancies between the observed rotation of galactic bodies and calculated predictions based on Kepler's laws. Ultimately, what we know from this evidence is that dark matter composes 80% or more[1] of the mass in our universe, but we have yet to directly detect it in any form. It is now the goal of many physicists to directly detect signatures of these elusive particles.

1.2 Indirect Evidence of Dark Matter

The indirect measurement of dark matter dates back to as early as 1933 [2]. Initial evidence was based on the orbital speeds of distant galactic bodies in the universe. A discrepancy was found by comparing these speeds to calculated predictions, signaling the existence of additional mass in the universe. The model used to map galactic rotational speeds was simple Keplerian mechanics based on Newtonian physics:

$$m\left(\frac{v^2}{r}\right) = G\frac{mM(r)}{r^2} \tag{1}$$

$$\Rightarrow v(r) = \sqrt{G\frac{M(r)}{r}}, \tag{2}$$

where $v(r)$ is the orbital speed of a body of mass m at radius r, $M(r)$ is the mass enclosed within radius r, and G is the gravitational constant.

This model predicts that the orbital speed of a body should decrease as $1/\sqrt{r}$. However, in the early 1900's, astronomers began to measure these rotational speeds by observing the redshifted radiation observed through the Doppler effect, and compiled them into datasets called rotation curves. They found that, despite the non-trivial distribution of real matter throughout the universe, the rotational speeds of galaxies did not follow the Keplerian model [3]. They in fact asymptotically trended towards what seemed like constants at high radii. This discrepancy is known as the "galactic rotation problem" and is one of the first indirect pieces of evidence for dark matter.

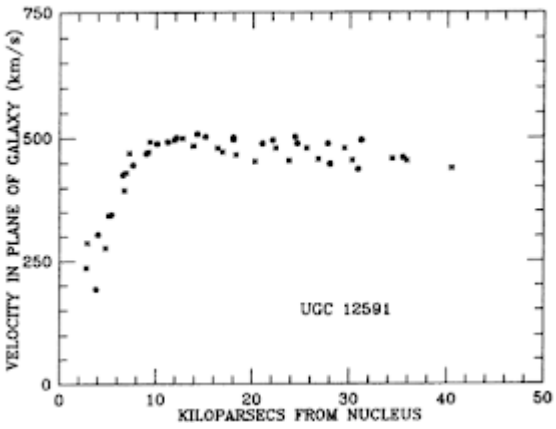

Figure 1: Original galactic rotation curve of UGC 12591 published by Vera C. Rubin in 1987. UGC 12591 was the "most rapidly rotating spiral disk known," and was strong evidence for the existence of additional unseen matter in the universe [3].

By the mid to late 1900's, many observational astronomers began to raise legitimate concerns regarding the accuracy of our understanding the universe due to this problem. In 1987, Vera C. Rubin published a rotation curve characterizing galactic cluster UGC 12591 (Figure 1). She commented on how exceedingly high the measured rotational velocities were. In her 1987 paper, she claimed that "it seems well established that field galaxies are embedded in massive, extended halos composed of nonluminous matter," referring of course to what would soon be accepted as dark matter [3].

Today we have accurate models for the distribution of dark matter which must exist to account for the discrepancy between the Keplerian model and the observed rotation curves (Figure 2) [4]. In the end, this *distribution* is all we actually know about dark matter. It describes where and in what concentrations dark matter must exist, but it says nothing about the nature of dark matter particles themselves. Determining any properties of dark matter at particles, such as their mass and size, is an open problem.

Theorists have created many promising dark matter models to solve these problems. Proposed first the 1980's, the current leading model is weakly interacting massive particles (WIMPs) [5]. The WIMP model suggests particles of mass roughly equivalent to a nucleon, $\mathcal{O}\ (1-1000\ GeV/c^2)$. As this parameter space becomes more thoroughly searched, many physicists have begun to shift their search to other candidates, such as sub-MeV "light" dark matter, or the much lighter ($\mathcal{O}\ \mu eV/c^2$) axion particle.

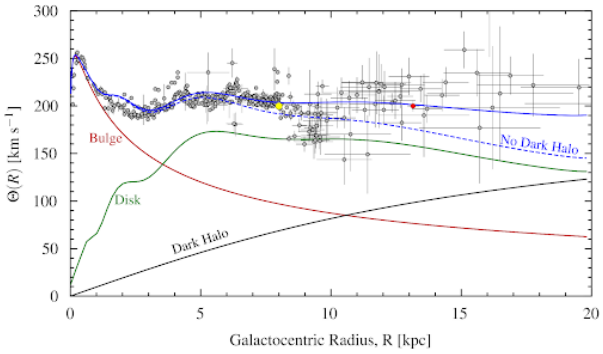

Figure 2: Unified Rotation Curve of the Galaxy. This curve decomposes contributions made by the bulge, disk, and dark matter halo of the Milky Way. From [4].

In reality, the feasible dark matter mass search range spans about 80 orders of magnitude, from ultralight bosonic dark matter as light as $10^{-22}\ eV$, to primordial black holes as heavy as $10^{48}\ GeV$[6]. As the life-cycle of a dark matter experiment often spans several years, it may take many more decades of progress to directly detect dark matter.

2 Low Temperature Detectors

A "low temperature detector" (LTD) typically refers to a sensor which operates best–or contingently–on a low operating temperature, typically below 77 Kelvin (LN). The development of new LTDs is an active research genre with a host of unique material science, physics, and engineering challenges. LTDs are extremely versatile and are used in a wide variety of applications ranging from medical use to particle astrophysics.

The detectors which are most relevant to our work are classified as either semiconducting detectors or superconducting detectors.

2.1 Semiconducting Detectors

A semiconductor is classified as a material with a small band gap between the valence and conduction bands. This allows for bound electrons in the valence band to jump to open states in the conduction band with the application of a small amount of energy. Most regular semiconducting materials have band gaps on the order of 1 eV. For example, the band gap for Si is 1.17 eV (0 K), and the band gap of high purity Ge is 0.74 eV (0 K) [7]. It is also possible to engineer semiconductors to influence their energy gaps by doping pure materials with impurities. For example, lithium doped silicon, Si(Li), has a band gap of 1.12 eV (0 K) [8].

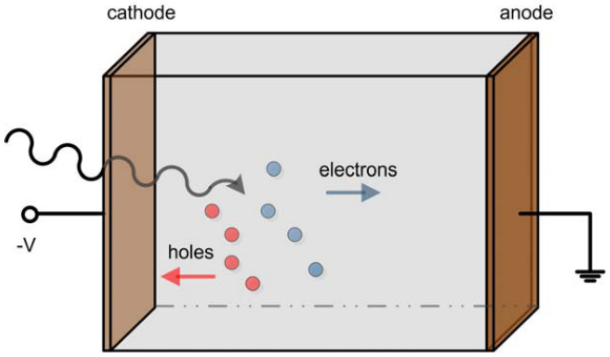

Figure 3: Generic mechanism for a planar semiconductor detector. Charge carriers produced from external interactions are drifted apart by a potential V. Mobilized charge carriers then generate a measurable signal. From [9].

A semiconductor detector is a type of LTD which operates by measuring the charge carriers produced from ionization events in semiconducting targets. When a particle interacts with the semiconductor, it deposits energy which creates electron-hole pairs in the semiconductor, and also creates phonons due to the vibrating lattice. Freed charge carriers are then collected by an electric field and measured as a current, voltage, or charge signal (Figure 3). It is advantageous to cryogenically cool the detector to thermally "freeze out" as many high-energy charge carriers as possible, as governed by Boltzmann statistics.

Material selection in semiconductor detectors include both the band gap of the material and the atomic number of the elements used. The atomic number of the material affects how the material interacts with other particles in collision events, and the band gap is directly related to the energy threshold and energy resolution of the detector.

The Search for Particles of Light Dark Matter with Narrow-Gap Semiconductors (SPLENDOR) collaboration is developing a light dark matter experiment featuring designer semiconductor materials with band gaps on the order of 1-100 meV [10]. The primary advantage of using narrow-gap semiconductors is that they are sensitive to much lower energy depositions than traditional semiconductors, but they can also require more complex readout and amplification technology to effectively operate in real world conditions.

2.2 Superconducting Detectors

Improvements in fabrication tools from the semiconductor industry have enabled the use of superconducting devices as low temperature detectors for over 40 years.

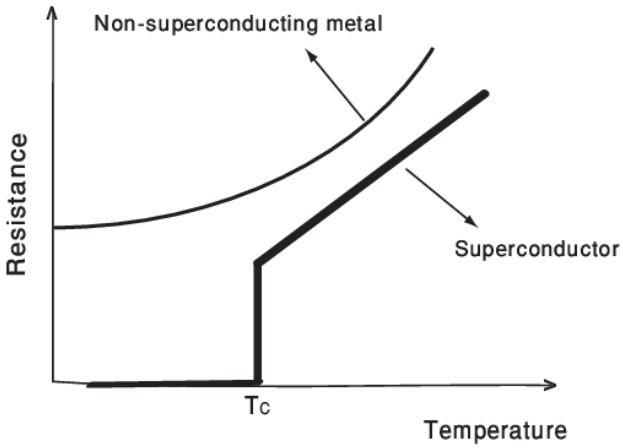

Figure 4: A resistance-temperature curve for a generic superconductor from [12]. The sharp increase in resistance corresponds to a phase transition from superconducting to normal at the critical temperature, T_c. When a device is biased within (or barely below) this phase transition, even small energy depositions that create small temperature rises can yield relatively large resistance changes in the material. This property of superconductors is exploited in many LTDs to maximize their energy sensitivity.

A superconductor is a material which, below a certain critical temperature, exhibits no electrical resistance as it carries current. Properties of these materials can be exploited to create clever detector devices, capable of measuring extremely small quantities of energy with high resolution.

Usually, the most difficult design challenges associated with any superconducting device are 1) fabrication process issues and 2) detector scalability and multiplexing. Desired energy sensitivity is another major factor which determines which detector design is best for a given application. Each detector design exhibits a unique set of trade-offs which must be considered when selecting a detector for any application.

2.2.1 Transition Edge Sensors (TESs)

Transition edge sensor (TES)-based detectors are a type of superconducting detector which operate by measuring the change in resistance of a superconducting material as it transitions from the superconducting to the normal state. A TES exploits the sharp phase transition profile of superconducting materials at their critical temperature to provide great sensitivity to miniscule changes in temperature (see Figure 4). These small changes in temperature are achieved with small energy depositions from external sources, such as ionizing radiation, cosmic rays, or other particles.

The behavior of thin-film superconductors near the superconducting transition is described by

Ginzburg–Landau theory [13]. At this transition, characteristics of the superconductor are strongly dependent on its Ginzburg–Landau parameter, which can be approximated as

$$\kappa \approx 0.715\ \lambda_L(0)/\ell(d)$$

where $\lambda_L(0)$ is the penetration depth at $T = 0$ (London penetration depth), and $\ell(d)$ is the electron mean free path [14]. This parameter determines which type of superconductor (I or II) a film will behave as, which primarily affects behavior at the critical temperature. For many particle astrophysics applications a type II superconductor is preferred, so materials with a higher κ (shorter mean free path) are chosen [14].

In many detector designs, TESs are made out of more than one superconducting material in order to optimize the efficiency of the detector. Aside from the thermometer material itself, the choice of absorber material is also critical to the performance of the detector. Choosing an absorber is highly influenced by the nature of the particle being detected. When detecting astro-particle interactions, such as dark matter, particles of interest first interact with a bulk target substrate. Energy from these interactions is converted into athermal phonons which propagate towards the surface film where they ideally get absorbed. The biggest challenge is sensing these phonons with high efficiency before they thermalize. Picking a material and design with a high phonon coupling efficiency is critical to the performance of the detector.

In this cross-section of constraints, tungsten and aluminum are common choices of detector and absorber materials, respectively. Other common TES materials include niobium, titanium, and tantalum.

2.2.2 Microwave Kinetic Inductance Detectors (MKIDs)

Microwave kinetic inductance detectors (MKIDs) are superconducting detectors that are most known for their ability to be easily incorporated into large arrays of high fill-factor. Fundamentally, an MKID is a tiny micro-resonator composed of an inductive and capacitive element. The physical geometry of each MKID when fabricated determines the frequency at which the MKID achieves resonance. Many MKIDs can patterned at once on the same wafer with slightly different resonant frequencies. When an incident particle interacts with the device, the surface inductance of one or more resonators will change slightly, pushing the resonance of that circuit to a lower frequency [15].

A continuous microwave tone is used to readout many MKIDs at once in the frequency domain. An off-resonance circuit will result in a notable absorptive dip at a specific frequency in Fourier space. This signature can be associated with a specific resonator, effectively providing spatial resolution for incident excitations.

The greatest advantage of MKIDs is native frequency-domain multiplexing thanks to their clever design. MKIDs are also regarded as relatively simple to fabricate and highly scalable, since many MKID designs can be made in just one fabrication layer. This is why they are popular for use in large focal planes of telescopes and other large-scale experiments demanding a high degree of multiplexing and good fill-factor.

3 Cryostats

There are many cryostat designs widely used for LTDs which can achieve temperatures below 4 Kelvin. Each kind of cryostat offers distinct advantages and disadvantages characteristic to the physics responsible for their functionality. The kind of cryostats regularly used in our experiments are dilution refrigerators and 3He adsorption refrigerators (Figure 5).

3.1 Dilution Refrigerators (DRs)

The most widely sought kind of cryostat today is the dilution refrigerator (DR). DRs typically boast impressive performance statistics, including base temperatures somewhere between 8 mK and 20 mK with respectable overall cooling power at these temperatures (Oxford ProteoxLX $\geq 25\,\mu$W @ 20 mK [16]). Modern DRs are relatively simple to operate since they do not require cryogen refills other than liquid nitrogen for a cold trap. DRs utilize a closed cooling loop with a carefully monitored mixture of 3He and 4He. The mix is thermodynamically manipulated in such a way as to slowly pump thermal energy continuously out of the base stage [17].

Once cold, a DR can maintain base temperature for months or years if desired. This makes a DR ideal for hosting long duration data-taking experiments, such as dark matter searches. The largest downfalls of DRs are their relatively high cost, which are upwards of half a million dollars, and their long cooldown times, which vary greatly depending on the thermal mass being cooled.

Figure 5: A 3He cryostat used for testing SPLENDOR readout electronics at SLAC national accelerator laboratory. Base temperature of ∼300 mK.

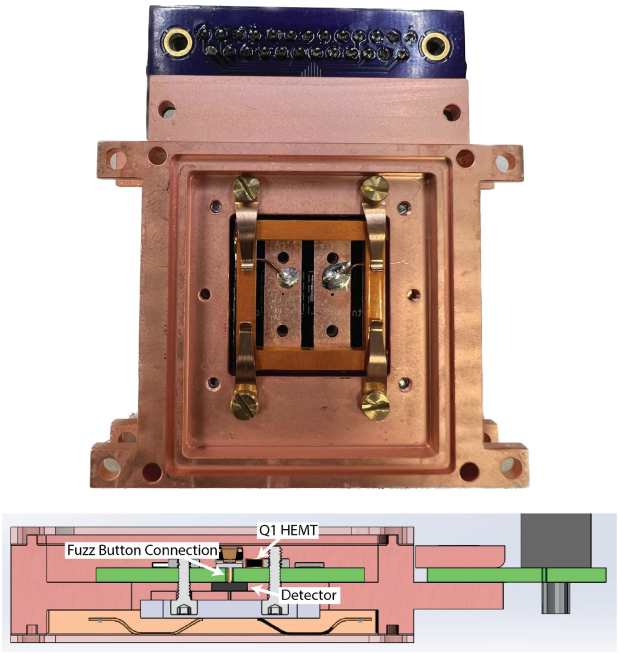

Figure 6: **TOP:** Backside picture of the prototype SPLENDOR detector housing with silicon test devices installed. **BOTTOM:** Cross-section CAD model of the SPLENDOR detector housing. Labeled are the detector crystal, front-end HEMT, and the fuzz button connection providing a low capacitance connection between the detector and the HEMT. From [10].

3.2 3He Adsorption Refrigerators

A 3He adsorption refrigerator (3He fridge) relies on the separate evaporative cooling of 3He and 4He achieve base temperatures around 300 mK. A 3He cryostat can maintain base temperature until the liquid pots run dry of helium (typically a couple of hours of operation at base temperature), at which point the system must be reset.

A 3He fridge can come in an open or closed loop variety. In closed loop designs, all of the helium (including the 3He) is recollected in adsorbent pots which are used to control the flow of 3He and 4He throughout the system. Even as closed systems, 3He fridges are largely deprecated due to the advent of DRs and adiabatic demagnetization refrigerators, but are still often seen in older infrastructures.

One major advantage is that a 3He fridge can be cycled from room-temperature to base-temperature significantly faster than many other cryostats, allowing for a much faster pace of R&D work. Their main disadvantage is that they typically do not hold base temperature for longer than several hours before needing to be cycled again.

4 SPLENDOR

The SPLENDOR (Search for Particles of Light Dark Matter with Narrow-Gap Semiconductors) collaboration is building a small prototype dark matter experiment targeting "light dark matter" in the sub-MeV mass regime. The two key components of the experiment are 1) the detector, which is under development by collaborators at Los Alamos National Laboratory; and 2) the amplifier, which our collaboration has been optimizing at SLAC for specific physics applications.

4.1 SPLENDOR Detector

The SPLENDOR detectors are designer narrow-gap semiconductor-type detectors [18]. Incident dark matter particles will scatter with the detector lattice, depositing small amounts of energy. If packets of energy are grater than the intrinsic band gap of the semiconductor, electrons will be excited from the valence band to the conduction band. Using an external electric field, these conduction electrons are drifted to a point contact to be read out as charge signals by the charge-integrating amplifier.

Given the nature of the particles we seek to detect using this scheme, a narrow band gap is desirable. The SPLENDOR detectors are designed to have a band gap on order of 1-100 meV. This is achieved by hand-growing crystals classified as zintl phase semiconductors through growth processes such as chem-

ical vapor transport and flux growth. These special crystals are designed and grown by researchers are Los Alamos National Laboratory. Assuming amply low-noise amplification, these detectors are capable of achieving sensitivity to light particle dark matter in the sub-MeV mass regime [10].

4.2 SPLENDOR Charge Amplifier

The SPLENDOR detector signals are read out using a two-stage amplifier that utilizes custom low-capacitance high electron mobility transistors (HEMTs) operable well below 4 Kelvin. The overall energy resolution, σ_E, of the SPLENDOR experiment is proportional to the energy gap of the detector crystals, E_{gap}, and the total input capacitance of the readout chain:

$$\sigma_E \propto E_{\text{gap}}(C_{\text{detector}} + C_{\text{input}} + C_{\text{parasitic}}) \quad (3)$$

where C_{detector} is the capacitance of the detector crystal, C_{input} is the capacitance coupled directly into the detector by the Q1 HEMT, and $C_{\text{parasitic}}$ is the parasitic capacitance of the rest of the readout chain. The amplifier's performance is improved by minimizing these parameters.

To do this, SPLENDOR uses special low-frequency (10 Hz – 1 MHz), low-noise, low-capacitance HEMTs commercially available from CryoHEMT. Like normal transistors, HEMTs can be configured in a common-source configuration to provide voltage gain, or in a voltage-follower configuration to act as a buffer element. Unlike normal transistors, HEMTs have exceptionally excellent noise performance, low power requirements, and can come in low capacitances models, making them ideal for use in low-noise cryogenic amplifiers. HEMTs feature a degenerate 2D electron gas layer which is utilized to achieve small on-resistances and high current densities, yielding high power densities [11]. This enables their operation at temperatures less than 4 K, below the freeze-out temperature of standard transistors.

Prior to our work, HEMTs had not been characterized for operation below 4 K. In Summer 2022, we successfully operated a HEMT at 360 mK in a 3He cryostat at SLAC, demonstrating that they can be used in our experiment (Figure 7). They have since been used in the SPLENDOR amplifier design to great success at temperatures as low as 10 mK.

The splendor detectors have extremely small capacitances by design, so $C_{\text{detector}} \sim \mathcal{O}(1pF)$ [10]. To minimize C_{input}, an amplifier with ultra low intrinsic capacitance is required. Finally, to minimize $C_{\text{parasitic}}$, it is best to entirely decouple the detectors from the rest of the readout chain using voltage-following transistors. These are the primary design criteria motivating the design of the SPLENDOR two-stage amplifier design.

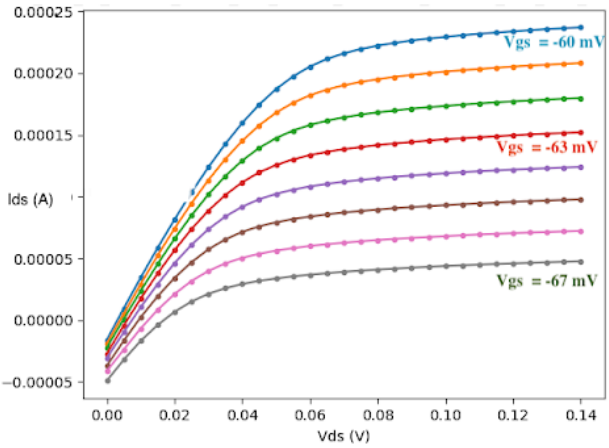

Figure 7: Characterization data of a HEMT exhibiting standard transistor modulation behavior at 360 mK in a SLAC 3He cryostat. This batch of HEMTs had previously been rated to operate only as low as 4 K.

The SPLENDOR amplifier design (Figure 8) utilizes a front-end HEMT ($C_{\text{input}} = 1.6pF$) in a voltage-follower configuration, coupled directly to the detector crystal to buffer the detector signal at 10 mK. This buffering is essential for decoupling the detector from the parasitic capacitance of the rest of the readout chain. With this configuration, $C_{\text{paracitc}} \approx 1pF$.

The buffered signal is then amplified by a second HEMT ($C = 200pF$) in a common-source configuration to provide a gain of 36 at 10 Hz. Since the detector signals are buffered by the front-end HEMT, this capacitance contributes minimally to the total input capacitance. The signals are then further amplified by room temperature amplifiers and filters before being digitized by a Moku:Pro [10].

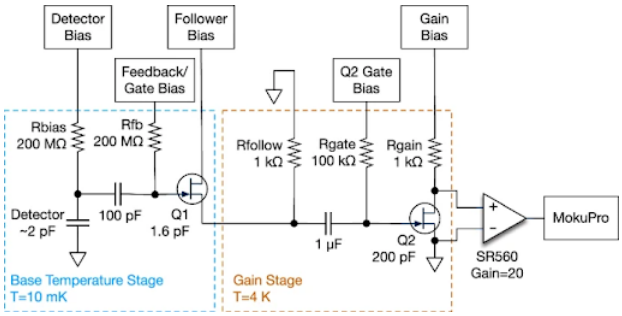

Figure 8: Simplified SPLENDOR amplifier circuit diagram. Charge produced within the detector is integrated onto Q1, which acts as a voltage buffer. The signal is amplified at the 4K gain stage and undergoes a further stage of room temperature amplification before digitization. The accrued charge on the Q1 gate is passively reset via the feedback resistor R_{fb} [10].

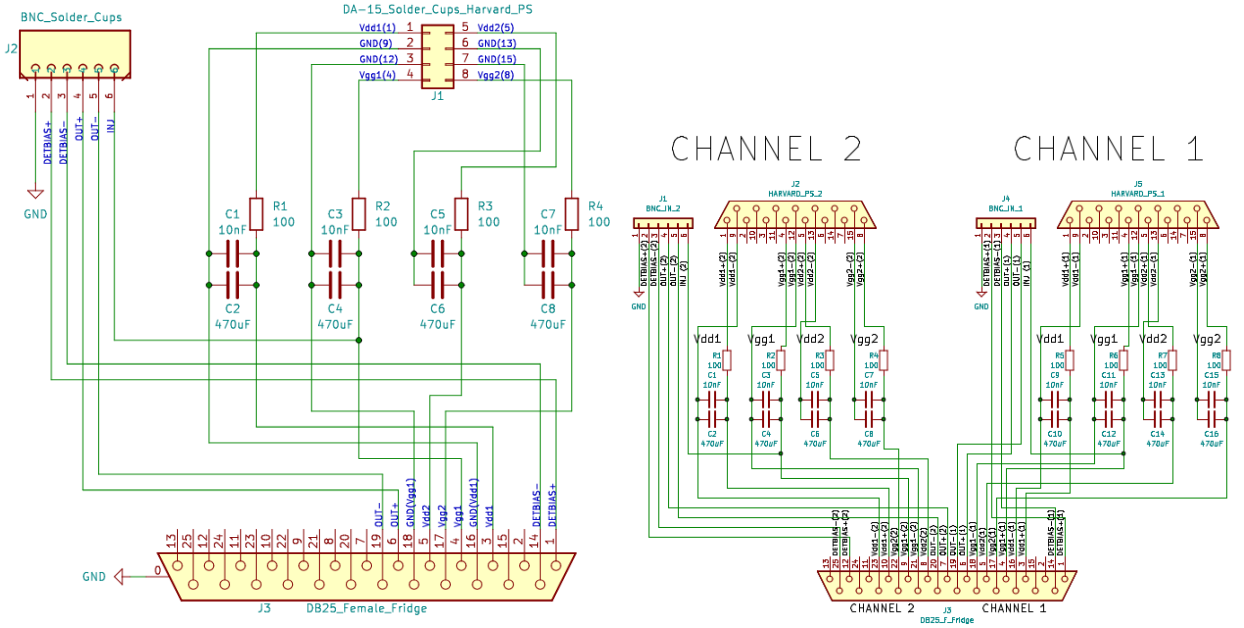

Figure 9: **LEFT**: Schematic of the Version 1 SPLENDOR filter board operated at room temperature. Passive RC filtering is composed of $R = 100\Omega$ and $C = 470\mu F + 10nF$. **RIGHT**: Schematic of the Version 2 SPLENDOR filter board. This design provides filtering for two, 2-stage amplifiers operated in parallel. It features the same passive RC filtering per-channel as version 1.

4.2.1 Room Temperature Filtering

Essential to the operation of the SPLENDOR amplifier is the need to provide clean DC bias signals to the HEMTs responsible for charge signal buffering and gain. We found that additional passive filtering was required to prevent 60Hz power line noise from from coupling to the detectors. To do this, we designed a custom filter board to be used in conjunction with the amplifier chain.

Our version 1 filter board (Figure 9, left) was designed with four separate DC bias lines, which was enough to operate two HEMTs (one 2-stage amplifier channel) simultaneously. We encapsulated the board in a metal box to prevent external electromagnetic noise from coupling to the DC bias lines. It was also designed to interface directly with the hermetic feed through port on the cryostat in order to minimize potential pickup through unshielded cables or leaky connectors.

The filter box utilized four simple RC filters with $R = 100\Omega$, $C = 470\mu F + 10nF$, each with a cut-off frequency of $f_{rc} = 3.39Hz$. This provided strong protection from any non-DC noise riding on the DC outputs from the power supply. It was important that the filter box interfaced directly with the cryostat to minimize the possibility of external radiation interfering with the DC signals before entering the cryostat.

Version 2 of the SPLENDOR filter board (Figure 9, right) was designed to accommodate two separate amplifier chains in parallel. Each channel was functionally identical to version 1, but there were twice as many channels to accommodate the readout of two simultaneous detectors in parallel.

4.3 SPLENDOR Amplifier Performance

The completed prototype charge amplifier was tested at SLAC National Accelerator Laboratory in an Oxford Proteox dilution refrigerator at a base temperature of 9.5mK. This preliminary version of the amplifier showcased a total estimated charge resolution of 7.2 electrons and total voltage gain of 36 at 10 Hz using an assumed total input capacitance of $5pF$ (see Figure 10). We are continuing wo work towards our goal of single-electron energy resolution by optimizing noise performance further. Currently, our greatest noise sources are pick-up from communication lines, pulse-tube cooler noise, and other environmental sources. We are working on improving the electromagnetic environment around the amplifier and experimenting with several measures to reduce ambient noise sources.

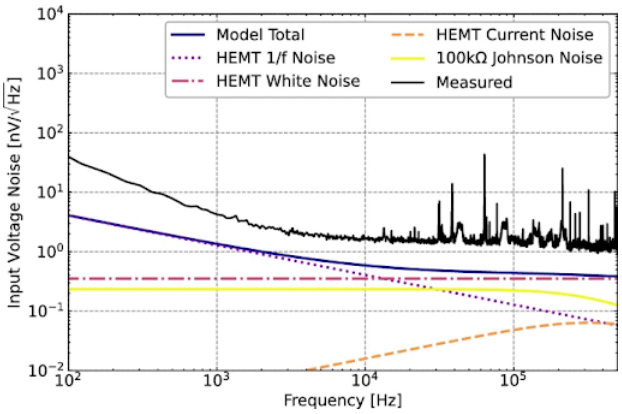

Figure 10: The measured amplifier voltage noise spectrum, with the base temperature board at 9.5mK. The high-noise floor is dominated by room temperature electronics coupling down to the input of the amplifier [10].

4.4 Custom Pick-n-Place Device for SPLENDOR

One challenge associated with using the delicate SPLENDOR detectors is mounting them with care and precision into custom machined copper housings. Doing this by hand is extremely difficult, time-consuming, and could lead to damage of the detectors. Additionally, hand mounting detectors is not a scalable solution which could be used in a larger experiment with more than a handful of detectors.

To solve this issue, I built a custom Pick-n-Place device for SPLENDOR capable of precisely mounting detectors quickly with minimal strain to the detectors (Figure 11). I began by disassembling a new Prusa Research i3 Mk3S+ 3D printer. I reused the existing stage motors, but added a new rotation stage to the print bed to get 4-axis spatial control in 3D space. A suction head powered by a controllable vacuum motor was added to reliably lift and release the detector crystals. An attached microscope camera allows the user to monitor the picking process in real time.

The existing Prusa xy-axis stepper motors come with ∼1 µm resolution, allowing for extremely precise placement our detectors into their housings during assembly.

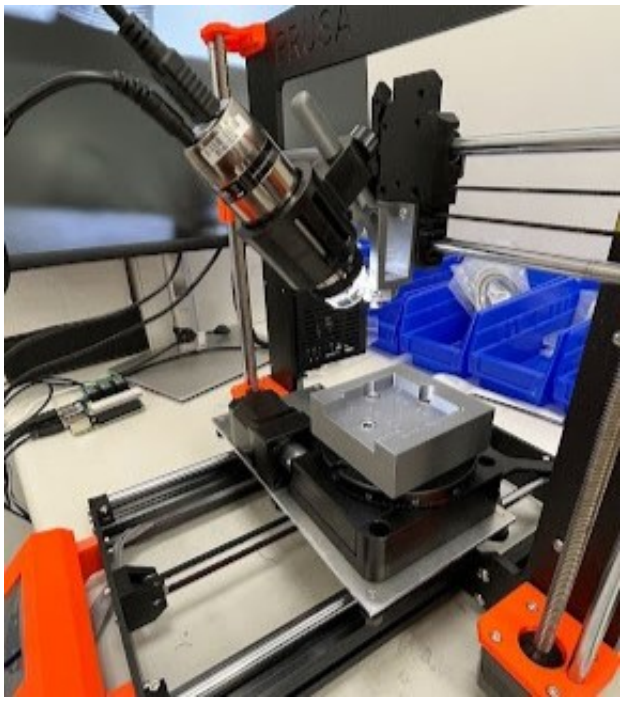

Figure 11: The pick-n-place device repurposed from a Prusa Research I3 Mk3S+. This apparatus readily enables accurate and precise mounting of fragile detectors in to complex detector housings.

MKIDs can also be used as dark matter detectors by measuring phonons coupled from a target substrate. Micro-resonators as low temperature detectors have many parallels to qubits for quantum computing, so research in novel resonator designs tap into many additional funding avenues available to quantum information science research goals.

MKIDs rely on the ability to precisely tune each individual detector's resonant frequency so they can be multiplexed in the frequency domain efficiently. Poorly manufactured MKIDs may suffer from collisions in frequency space, which can make it impossible to distinguish signals from different detectors. This places constraints on the acceptable level of manufacturing error in the fabrication process.

In order to aid this process, we have characterized several of these devices using a scanning electron microscope (SEM) available at the Center for NanoStructures at SCU.

5 MKID Development

Microwave kinetic induction detectors (MKIDs) are LTDs frequently used in cosmology applications. MKIDs have the advantage of native frequency-domain multiplexing, allowing for easy instrumentation and a much greater fill factor on a focal plane than other kinds of detectors (see section 2.2.2).

5.1 Nanofabrication

Superconducting devices relying on quantum-mechanical properties of superconductors, such as the Josephson effect or perturbations in surface inductance, are too small to be manufactured by hand. Instead, these devices must be fabricated with photolithography in a nanofabrication lab.

Photolithography is a process used to pattern thin films on a substrate. The process begins with a clean wafer, which is then coated with a thin film of the material to be patterned. The wafer is then coated with photoresist. The photoresist is exposed to UV light through a mask which is designed to block light in certain areas. In modern times, maskless exposure tools such as the Heidelberg MLA 150 are capable of exposing photoresist with sub-micron resolution without the use of a mask, which speeds up R&D times greatly. Exposure hardens the photoresist in the areas exposed to light, preventing it from being removed by the developer or etchant.

Then, the wafer is developed, which removes the photoresist in the areas not exposed to light. Afterwards, the wafer is etched, which removes the film wherever it is not protected by hardened photoresist. Finally, the wafer is cleaned and the photoresist is removed, leaving behind the patterned thin film.

This process is capable of producing devices with micron-scale (or even smaller) feature sizes, including modern MKIDs and similar superconducting energy sensors.

Hardly ever are new fabrication processes successful the first time. It is common for new fabrication processes to require many iterations of testing and adjustment before a successful device is produced. To diagnose problems in the fabrication process of our MKIDs we performed SEM imaging.

5.2 SEM Metrology

A scanning electron microscope (SEM) is a tool used to image features as small as $\sim 1\,\text{nm}$. An SEM works by scanning a focused beam of electrons across a sample and counting the reflected (backscattered) and ionized (secondary) electrons from the sample. The intensity of these electrons is then used to create an image of the sample's surface.

I performed SEM imaging of 2 batches of MKID devices fabricated at Stanford Nanofabrication Facility (SNF) to better understand fabrication-related device failures. Our MKID design includes a 300 nm-thick patterned Nb feedthrough layer that is covered with a 30 nm layer of Al in a subsequent deposition. The Al is then patterned into the resonator structures that define a specific MKID geometry. Initial measurements with the MKID-based detectors revealed poor superconducting transition reliability, indicating critical fabrication issues. We observed the samples under the SEM in order to understand what part of the fabrication process might have caused these particular devices to fail.

In our fist set of test devices, only the niobium layer was patterned. Under the SEM, we found several instances where it appeared like the Nb film was

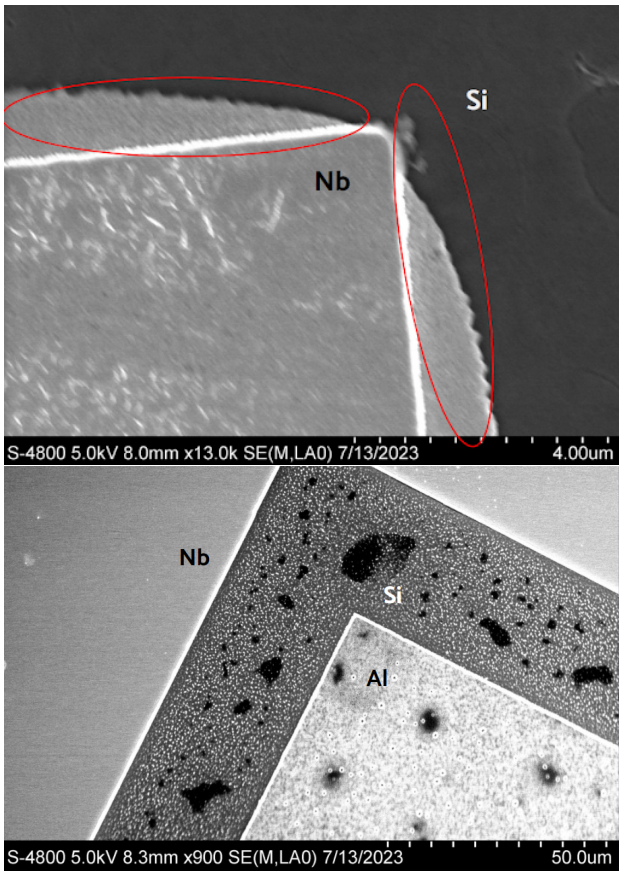

Figure 12: SEM images of two prototype MKID samples under development at SLAC. **TOP**: Patterned Nb on Si. The Nb film appears underetched, leaving bulged edges contributing to sloppy trace geometry. **BOTTOM**: Post Al patterning. Pitting left behind is from poor selectivity from the Al etch step.

underetched, as shown in Figure 12 (top). This significantly changed the geometry of the resonators, causing them not to function as intended.

A second sample from after the aluminum was pattered was observed in SEM (Figure 12, bottom). We found severe pitting in the thin aluminum film and the Si substrate behind it. We concluded that the aluminum etch step was severely over-etching the device, causing damage to the rest of the substrate.

Overall, we determined that the selectivities of the dry etchants used ($BrCl_3$ and Cl_2) were inadequate to properly etch the desired features of the device in both samples investigated. This insight contributed to adjusting the process used to fabricate these devices.

Figure 13: The Fridge Manager application developed for the 3He cryostat at SLAC. The GUI provides a user-friendly interface for monitoring and controlling the cryostat from any web browser. The graph shows the temperature of every stage of the cryostat over time, and can also display pressure and voltage data. The GUI allows the user to control data logger settings and remotely perform a fridge cycle.

6 Cryostat Control GUI

6.1 3He Cryostat Operation

The manual operation of a 3He cryostat requires significant expertise due complexities in the thermodynamic cycle used to achieve base temperatures near 300 mK. First, the cryostat must be sealed and pumped down to vacuum. Air left in the vacuum chamber has a possibility of condensing on the inner walls and critical structure of the cryostat, which presents a strong possibility of damage.

To get cold, the SLAC 3He cryostat first utilizes a pulse-tube cooler to achieve a stable temperature of ∼4 K. To get any colder than 4 K, the fridge must be "cycled" by applying certain voltages to various heaters and gas-gap switches at the right moments in time. When run normally, the cold stage of the fridge will then cool to ∼ 300 mK over a period of ∼1 - 4 hours (the longer run time corresponds to the first cycling of the fridge at the start of a run). It will remain at this temperature for ∼8 hours of experimental run time. Subsequent cycles of the 3He fridge sample stage only require ∼1 hour to go from 4 K back to ∼ 300 mK.

6.2 Development of the Fridge Manager Application

The manual procedure for cycling the 3He fridge is complex and requires proper manual control of various heating elements in the cryostat. At SLAC, we had previously performed this procedure manually by logging into the cryostat computer and running a series of scripts to cycle the fridge. This process was either completed in-person at the cryostat, or while logged into the fridge computer remotely, which locked other users out from seeing the status of the fridge.

To improve this process, colleague Makar Dubovskov and I developed a "Fridge Manager" web-based application which interfaces directly with the cryostat (Figure 13). The application was split into 3 parts: the front-end GUI, the back-end server, and the cryostat control server. The front-end GUI and back-end server were both written as unified Python Streamlit application. The cryostat control server was a separate Python script which interfaced directly with the cryostat hardware.

The back-end requests information from the cryostat server, which reports stage temperatures, gauge pressures, and heater voltages. It presents this information in a neatly organized front-end graphical user interface (GUI), which provides the user with this critical telemetry data from the cryostat. The GUI enables users to view this data from any device on the network. Additionally, it allows the user to operate the cryostat and perform a fridge cycle remotely from any device. The cryostat server logs all of the telemetry data and saves it permanently for future reference. This GUI has enabled our team to use this cryostat much more efficiently than ever before.

7 Conclusion

In this thesis I presented some of the collaborative cryogenic detector-related work I performed with professional physicists from SCU and SLAC. My work focused mostly on these key areas: 1) the development of a custom filter board for the SPLENDOR charge amplifier, 2) the characterization of MKID devices using SEM metrology, and 3) the development of a graphical user interface for cryostat con-

trol. The work I performed in these areas is still impacting the ongoing laboratory efforts in the DMQIS labs at SLAC. By working as a team and leveraging my unique abilities and skills, I was able to make significant contributions to the development of these projects.

Acknowledgements

This work was supported in resources and equipment by the Santa Clara University Department of Physics, SLAC National Accelerator Laboratory, Stanford University, and the Kavli Institute for Particle Astrophysics and Cosmology. This work was funded by a Geoff and Josie Fox Summer Research Fellowship. I thank Dr. Betty Young for her genuine guidance and support in this project, and Dr. Noah Kurinsky for his additional mentorship and program support.

References

[1] S.D.M. White, M.J. Rees, *Mon. Not. R. Astron. Soc.*, **183**, 341-358 (1978).

[2] F. Zwicky, *Helvetica Physica Acta*, **6**, 110-127 (1933).

[3] V.C. Rubin, *Proceedings of the 117th. Symposium of the International Astronomical Union*, **117**, 51 (1987).

[4] Y. Soufe, M. Honma, T. Omodaka, *Publ. Astronom. Soc. Japan*, **61**, 227-236 (2009).

[5] P.J.E. Peebles, *Astrophysical Journal*, **263**, L1-L5 (1982).

[6] C. Csaki, A. Ismali, s. Lee, *J. High Energ. Phys*, **2023**, 53 (2023).

[7] C. Kittel, *Introduction to Solid State Physics*, 8th ed. P190 (2005).

[8] M. Schieber, J.C. Lund, R.W. Olsen, D.S. McGregor, J.M. Van Scyoc, R.B. James, E. Soria, E. Bauser, *Nucl. Instr. and Meth. in Phys. Res. A*, **377**, 492-495, (1996).

[9] Q. Zhang, C. Zhang, Y. Lu, K. Yang, Q. Ren, *Sensors*, **13**, 2447-2474 (2013).

[10] J. Anczarski et al, *J. Low Temp. Phys.*, **214**, 256-262 (2024).

[11] X. Ding, Y. Zhou, J. Cheng, *CES Transactions on Electrical Machines and Systems*, **3**, 54-64 (2019).

[12] A. Khalid, R. Salman, S. Anwar, *Principles and Applications of Superconducting Quantum Interference Devices (SQUIDs)* lab manual, (2010).

[13] V.L. Ginzburg, L.D. Landau. *Zh. Eksperim. i Teor. Fiz.*, **20**, 1064 (1950).

[14] K. Irwin, G.C. Hilton, *Topics Appl. Phys.*, **99**, 63-149 (2005).

[15] P. Day, H. LeDuc, B. Mazin, A. Vayonakis, *Nature*, **425**, 817-821 (2003).

[16] Oxford Instruments NanoScience, *Oxford ProteoxLX Brochure*, (2022).

[17] G. Batey, G. Teleberg, *Principles of Dilution Refrigeration*, (2015).

[18] S. Watkins *Searching for Light Dark Matter with Narrow-gap Semiconductors: The SPLENDOR Experiment*, UCLA DM poster LA-UR-23-22869, (2023)

[19] S. McHugh, B. Mazin, B. Serfass et al, *Rev. Sci. Instrum.*, **83**, 044702 (2012).

[20] J.G. de Swart, G. Bertone, J. van Dongen, *Nature Astronomy*, **1**, (2017).

[21] F. Zwicky, *Astrophysical Journal*, **86**, 217 (1937).